Remote drying in the North Atlantic as a common response to precessional changes and CO_2 increase over land

Patrick Kelly,[1] Ben Kravitz,[1] Jian Lu,[1] and L. Ruby Leung[1]*

[1]Atmospheric Sciences and Global Change Division, Pacific Northwest National Laboratory, Richland, WA

[*]To whom correspondence should be addressed: P.O. Box 999, MSIN K9-24, Richland, WA 99352, USA. E-mail: patrick.kelly@pnnl.gov.

Revised for publication in *Geophys. Res. Lett.*

Key Points

- CMIP5 mid-Holocene and AMIP4XCO2 simulations exhibit similar energy, circulation, and rainfall changes in the NH summer subtropics
- Local CO_2 and insolation increase near North Africa reproduce the total pattern of the response to global forcing
- Direct forcing from insolation and CO_2 yield a similar response due to the common importance of land heating on stationary wave changes

Abstract

Here we demonstrate that changes of the North Atlantic subtropical high (NASH) and its regional rainfall pattern during mid-Holocene precessional changes and idealized 4xCO_2 increase can both be understood as a remote response to increased land heating near North Africa. Despite different sources and patterns of radiative forcing (increase in CO_2 concentration vs. changes in orbital parameters), we find that the pattern of energy, circulation, and rainfall responses in the Northern Hemisphere summer subtropics are remarkably similar in the two forcing scenarios because both are dominated by the same land-sea heating contrast in response to the forcing. An increase in energy input over arid land drives a westward displacement of the coupled NASH-monsoon circulation, consistent with increased precipitation in the Afro-Asia region and decreased precipitation in the America-Atlantic region. This study underscores the importance of land heating in dictating remote drying through zonal shifts of the subtropical circulation.

1. Introduction

Rainfall is a key variable that connects climate to its socio-economic impacts. Near subtropical North America, rainfall is strongly influenced by the position of the subtropical high, whose winds dictate mean moisture pathways in addition to the steering of tropical cyclones (Colbert and Soden, 2012). The North Atlantic subtropical high (NASH) shifts westward in future climate change projections (Shaw and Voigt, 2015). Similarly, the NASH was displaced westward during the mid-Holocene period (6kya), consistent with a drier North American climate (Mantsis et al., 2013; Shin et al., 2006; Grimm, 1993). We seek a unified understanding of what drives these similar changes in the NASH and its rainfall pattern under different climate forcings.

Heating from monsoon precipitation plays a fundamental role in the formation and maintenance of the anticyclonic flow of the subtropical high in the present-day climate (e.g. Rodwell and Hoskins, 2001; Chen et al., 2001). Under future climate change scenarios, monsoon precipitation is generally expected to increase due to CO_2 increase (IPCC *Climate Change, 2013)*. Relatedly, a variety of paleoclimate proxy reconstruction data (Jolly et al., 1998; Overpeck et al., 1996) and modeling evidence (Perez-Sanz et al., 2014; Harrison et al., 2015) also suggest that the monsoons of North Africa and Asia were significantly wetter during the mid-Holocene period due to orbital precessional changes.

The primary effect of increased insolation in the Northern Hemisphere (NH) during the mid-Holocene was to enhance land-sea energy asymmetries in summer via direct radiative forcing over land, thereby strengthening the North African and Asian monsoon, with oceanic and vegetative feedbacks playing a secondary role (Harrison et al., 2015). Similarly, CO_2 direct radiative forcing strengthens the Asian summer monsoon via increased land heating in prescribed-SST AGCM studies (Shaw and Voigt, 2015, 2016).

Given this similar role of increased land heating on monsoon strength in the NH, c*an we interpret the response of the coupled monsoon-NASH circulation to direct CO_2 forcing and direct insolation forcing in an analogous way?* Here we demonstrate– using CMIP5 analysis and spatially dependent radiative forcing experiments (Methods)– that the response of the NASH and its regional rainfall pattern are governed by the common mechanism of direct radiative forcing of remote arid land in 4xCO_2 and mid-Holocene experiments.

2. Methods

2.1. CMIP5 output

We used monthly output from the Coupled Model Intercomparision Project phase 5 (CMIP5; Taylor et al., 2012) from all available models that participated in the prescribed-SST AMIP and AMIP4xCO_2 experiments, as well as the coupled mid-Holocene and preindustrial control (piControl) experiments (Table S1 in Supporting Information). A detailed description of these experiments is found in Taylor et al (2012). We used a single ensemble member for each model participant and took the climatological June-August (JJA) average calculated over years 1979-2008 in the AMIP simulations. In the coupled simulations, we used the long-term climatological output, calculated over a sample of ≥100 years after sufficient model spin-up. Model data are first regridded to a standard 1.9°x2.5° horizontal grid before calculating a multi-model ensemble average. Data is obtained on 17 standard pressure levels from 1000-10 hPa. Any data points below ground are filled using a Poisson relaxation technique. In Figures 1-3, a "robust" grid point is defined as where >80% of models agree on the sign of the response.

2.2. Non-uniform 4xCO_2 in CAM4 and insolation increase in CCSM4

To identify the remote response in the western Atlantic to radiative forcing near North Africa, we repeated the AMIP4xCO_2 and mid-Holocene experiment of CMIP5 using the CAM4/CCSM4 (Gent et al., 2011; Neale et al., 2011) model, but with the respective CO_2 quadrupling and insolation perturbations applied only over the rectangular domain of 15°W-60°E longitude and 15°N-30°N latitude. This arid patch near North Africa was chosen because it represents the maximum in anomalous top-of-the-atmosphere (TOA) forcing and net atmosphere energy input anomalies as identified in the CMIP5 archive (Figs. S1-S2).

CO_2 concentration in the CAM4 model is prescribed as a constant value, column-by-column over the global grid, allowing the application of a simple horizontal spatial mask to achieve a non-uniform 4xCO_2 distribution (as in Shaw and Voight, 2016;

hereafter SV16). CO_2 is prescribed at 1392 ppmv over the domain 15°W-60°E and 15°N-30°N. Everywhere else, it is held to a nominal present day value of 348 ppmv. We do not apply any smoothing or tapering at the edges of the forcing domain. The simulation follows the standard AMIP protocol in all other respects. This experiment is called 'CAM4_AMIP4xCO_2_PATCH.'

To mimic the precessional-forced insolation change in the CMIP5 mid-Holocene (6kya) experiment, but over a zonally non-uniform domain (15°W-60°E; 15°N-30°N), we modify the radiation calculation of the CAM4 physics module in the coupled CCSM4 model to allow for spatio-temporal variations in insolation, rather than being prescribed by a solar constant. These variations are taken directly from the PMIP protocol (https://pmip2.lsce.ipsl.fr/design/tables/inso_tables_6k.shtml) and are prescribed as monthly anomalies on top of the present-day values. This yields an annual cycle of insolation over the forcing domain identical to that found in the standard CMIP5 mid-Holocene simulation, with a mean JJA insolation anomaly in the forcing region of about +20.3Wm^{-2}. Standard piControl insolation is prescribed everywhere else. Orbital parameters are set to their piControl values. All other boundary conditions and configurations (e.g. atmospheric gas concentrations, vegetation type, initial conditions, spinup, etc.) follow the standard mid-Holocene experimental design (Taylor et al., 2012). This experiment is called 'CCSM4_mid-Holocene_PATCH.'

2.3. Net atmosphere energy input

Forcing in this study comes in the form of perturbations to the *TOA* radiation budget, whether through CO_2 or insolation increase. This forcing can in turn perturb the energy balance of the atmosphere through its relation to net atmosphere energy input (*AEI*), defined as the difference between the *TOA* radiation budget and that at the surface:

$$AEI = TOA - SW - LW + SHF + LHF \quad , \qquad (1)$$

where *TOA* is defined positive downwelling, surface shortwave (*SW*) and longwave (*LW*) fluxes are positive downwelling, and sensible (*SHF*) and latent (*LHF*) heat fluxes are positive upwelling into the atmosphere. In regions where the surface energy budget approaches zero (e.g., over land), perturbations to *TOA* forcing can directly perturb *AEI* and act as a moist static energy source.

2.4. Moisture budget decomposition

Regional rainfall is the main impact variable of this study. We decompose a simplified column-integrated moisture budget to identify the source of regional rainfall changes under different climate scenarios, with an emphasis on the role of the stationary eddy circulation.

Beginning with the standard balance equation for water vapor under steady state:

$$\overline{P-E} \approx \frac{-1}{g\rho_w}\int_{sfc}^{toa} (\nabla\cdot\overline{\boldsymbol{v}q})\,dp \quad , \qquad (2)$$

the moisture transport term $\overline{\boldsymbol{v}q}$ in can be decomposed into terms relating to transient eddy, stationary eddy, and zonal mean circulation components:

$$\overline{\boldsymbol{v}q} = \underbrace{\overline{\boldsymbol{v}'q'}}_{transient} + \underbrace{\overline{\boldsymbol{v}}^{*}\overline{q}}_{stationary} + \underbrace{[\overline{\boldsymbol{v}}]\overline{q}}_{zonal} \quad . \qquad (3)$$

where overbars indicate a JJA climatological average, square brackets indicate a zonal average, an asterisk indicates a zonal deviation, and a prime indicates temporal deviation from the JJA climatology. In the discrete approximation of (2), we vertically integrate from 1000-10hPa utilizing the standard available pressure levels in CMIP5. This level of accuracy is sufficient for our purpose as we are interested in bulk rainfall changes between different climatic states averaged over the western Atlantic basin.

All terms of (3) are shown in the accompanying Supporting Information (Fig. S3) for the multi-model ensemble mean difference of AMIP4xCO_2 minus AMIP and mid-Holocene minus piControl. Since necessary fields at daily resolution were not commonly available in CMIP5 data to explicitly compute transient eddy moisture flux, the contribution from transient eddies is implicitly included as part of the budget residual (Figs. S3, S7).

Changes in the stationary eddy flux $\overline{\boldsymbol{v}}^{*}\overline{q}$ is the key term, so we further decompose it below (Fig. 3) to parse the total change into its ‘thermodynamic’ (i.e.

changes in humidity) and 'dynamic' (i.e. changes in the wind field) contributions (Seager et al., 2010):

$$\underbrace{\langle \delta (\nabla \cdot \overline{\boldsymbol{v}}^{*} \overline{q}) \rangle}_{total} = \underbrace{\langle \nabla \cdot (\overline{\boldsymbol{v}}^{*} \cdot \delta \overline{q}) \rangle}_{thermodynamic} + \underbrace{\langle \nabla \cdot (\delta \overline{\boldsymbol{v}}^{*} \cdot \overline{q}) \rangle}_{dynamic} , \quad (4)$$

where δ represents the experiment minus control JJA mean change and angled brackets indicate a column mass integration.

3. CMIP5 mid-Holocene and AMIP4xCO2 comparison

The June–August (JJA) net atmosphere energy input in the NH subtropics in response to a 4xCO_2 increase and mid-Holocene precessional changes in CMIP5 models is strikingly similar (Fig. 1, top row), despite significantly different model configurations and forcings: AMIP4xCO_2 simulations were forced by a globally uniform quadrupling of CO_2 under a fixed-SST constraint, whereas mid-Holocene simulations used a fully-coupled ocean model with interactive SSTs, forced by orbital changes resulting in a zonally uniform but latitudinally varying pattern of insolation change (Methods). Perturbations to TOA radiative flux (Figs. S1-S2) from these two different forcing scenarios result in a similar pattern and magnitude of net atmosphere energy input, with an increase over most land areas and a decrease over oceans, increasing land-sea heating asymmetry. Over land, the largest increase in net atmosphere energy input is over the arid subtropical region near North Africa, where cloud and water vapor masking have little influence (Merlis, 2015; SV16). Over subtropical ocean, a reduction in latent heat flux acts to compensate the positive TOA anomalies (Figs. S1- S2), leading to small or net negative (i.e., upward) atmosphere energy changes (Allen and Ingram, 2002).

Atmosphere energy input can be related to the divergent circulation and convection through the moist static energy framework (Neelin and Held, 1987), where positive energy anomalies imply low-level convergence and rising motion. In 4xCO_2 and mid-Holocene simulations, precipitation increases over tropical land and decreases over tropical ocean in the Eastern Hemisphere (Fig. 1, 2nd row), indicative of a strengthening of the continental African and Asian monsoons systems and a northwest shift of broad-scale tropical precipitation. The pattern of these regional rainfall changes is consistent with increased energy input over land and decreased energy input over the ocean (Fig. 1, top row), noting that the relationship between energy input and precipitation is not strictly local in monsoon systems, with maximum precipitation occurring slightly equatorward from the maximum in energy input (Nie, Boos, and Kuang, 2010). In both sets of simulations, low-level velocity potential is increased near 45°E (Fig. 1, 3rd row), indicating anomalous large scale low-level convergence over the Middle East, consistent with the increase in energy input there. This also corresponds to a westward displacement of the anticyclonic flow of the NASH near the surface into North American longitudes (Fig. 1 bottom row), as the rotational flow in the Atlantic is coupled to the divergent monsoon circulation to its east via Rossby wave dynamics (Rodwell and Hoskins, 2001; Rodwell and Hoskins, 1996).

Climatological heating from monsoon precipitation drive dynamical changes in the zonally asymmetric– or stationary wave– circulation, with monsoon heating acting as the primary control of the global stationary wave pattern in summer (Hoskins and Rodwell, 1995; Ting, 1994). At subtropical latitudes, the response to heating perturbations is largely baroclinic, so that the asymmetric circulation responses in the upper and lower troposphere are of opposite signs. In the climatological mean, the summertime anticyclonic flow of the NASH is coupled to an upper-level cyclone (vorticity source) and deep layer subsidence over the relatively cool eastern Atlantic (Miyasaka and Nakamura, 2005). But under the externally forced climate scenarios considered here, continental monsoon rainfall is increased, and a westward displacement of the entire vertically-coupled stationary zonal wave #1 pattern is seen (Fig. 2).

In both 4xCO_2 and mid-Holocene cases, the upper-level clockwise flow around the Tibetan anticyclone shifts poleward and extends further west into the Atlantic (Fig. 2 top, middle rows), consistent with poleward and westward shifts in precipitation (Fig. 1). In the eastern Atlantic basin, there are positive upper-level vorticity anomalies centered near 50°N corresponding to the northwest corner of the Tibetan anticyclone (Fig. 2, top row). This also results in positive vorticity anomalies extending further westward into the western Atlantic and Gulf of Mexico, given the characteristic southwest-northeast phase tilt of the upper-level stationary wave. The mass convergence implied by this upper-level vorticity anomaly is consistent with deep-layer subsidence around 100-60°W (Fig. 2 bottom row), as dictated by mass continuity. Increased CO_2 and insolation thus cause a coherent westward shift of the vertically-coupled baroclinic stationary wave circulation, consistent with subsidence-induced drying in the western Atlantic (Fig. 2, bottom row; Fig. 1, 2nd row).

While the pattern of these circulation changes is very similar in the subtropical western Atlantic, mid-Holocene changes are generally of weaker amplitude, despite comparable increases in energy input and monsoon rainfall to the east (Fig. 1). This may be due to SST warming in the coupled mid-Holocene simulations which partially weakens the land-sea heating asymmetry, and possibly model sampling differences (Table S1).

We decompose JJA precipitation minus evaporation *(P – E)* using a simple moisture budget (Methods) to directly connect changes in the circulation with regional rainfall changes. Summer drying in the western Atlantic in response to CO_2 and insolation increases can both be understood almost entirely in terms of changes in the stationary wave pattern, as the NASH and its deep-layer subsidence shift westward under increased land heating (Figs. 1, 2), causing low-level moisture flux divergence (Fig. 3). Stationary eddy moisture divergence $\nabla \cdot \overline{\boldsymbol{v}}^{*}\overline{q}$ is the primary budget term (See Fig. S3 for full budget). Further partitioning $\nabla \cdot \overline{\boldsymbol{v}}^{*}\overline{q}$ into changes due to the asymmetric circulation (i.e. 'dynamic' effect) and changes due to humidity (i.e. 'thermodynamic' effect; see Seager et al., 2010), clarifies the asymmetric circulation as the cause of basin-scale drying in the western Atlantic (Fig. 3). The thermodynamic term does play a more significant role in the local increase of precipitation, however. Increased humidity and increased convergence over land act in concert to drive strongly positive *P – E* changes in monsoon regions. But humidity changes are of minor significance to the negative *P – E* changes over the ocean. These results are common to both fixed-SST AMIP4xCO_2 simulations and coupled mid-Holocene simulations, and are consistent with recent work emphasizing the role of stationary eddies on the hydrological cycle in a warmer climate (e.g. Wills et al., 2016; Levine and Boos, 2016; Shaw and Voigt, 2015).

4. Response to spatially non-uniform radiative forcing

To better understand what drives these similar changes in the NASH and its rainfall pattern under various climate forcings in the CMIP5 archive, we next turn to idealized model experiments with the fully coupled Community Climate System Model version 4 (CCSM4; Gent et al., 2011) and its uncoupled atmosphere component (CAM4; Neale et al., 2011). CCSM4 and CAM4 are generally representative of the robust CMIP5 multi-model mean response to 4xCO_2 increase and mid-Holocene insolation changes shown in Figures 1-2. (see Figs. S4-S5). We used dedicated forcing experiments with spatially dependent CO_2 and insolation increases in CAM4 and CCSM4, respectively (Methods). Denoted ‘CAM4_AMIP4xCO_2_PATCH’ and ‘CCSM4_mid-Holocene_PATCH’, these experiments were forced by the same respective CO_2 and insolation perturbations as the CMIP5 experiments, but only over a patch of arid land on the northwest margins of the African and Asian monsoons (15°W-60°E and 15°N-30°N; see box in Fig. 4) where TOA and net atmosphere energy input anomalies are maximized (Figs. S1-S2). PATCH experiments are designed to verify that the NASH displacement and rainfall reduction in the western Atlantic (Fig. 1) can be interpreted as a remote response to anomalous energy input over arid land under increased CO_2 and insolation scenarios.

Figure 4 shows the energy, circulation and rainfall responses in CAM4_AMIP4xCO_2_PATCH and CCSM4_mid-Holocene_PATCH, plotted on the same color scale as Figures 1-2 to facilitate comparison with the CMIP5 multi-model response. In short, the response in CAM4_AMIP4xCO_2_PATCH and CCSM4_mid-Holocene_PATCH are very similar (Fig. 4), both to each other and to their standard AMIP/mid-Holocene counterparts using global forcing (Figs. S4-S5). The PATCH experiments also reproduce the same pattern as the robust multi-model mean CMIP5 response (Figs. 1, 2), albeit with smaller magnitude of changes in most fields. This may reflect secondary contributions of radiative forcing from other regions in amplifying the principal response, in addition to individual model differences.

Results from PATCH forcing experiments confirm the role of increased energy input over land near North Africa in driving a broad-scale enhancement of Afro-Asian precipitation and remote energy and circulation changes in the Atlantic via shifts in the global-scale stationary wave pattern. Radiative forcing of land near North Africa causes remote energy flux divergence over the ocean in the western Atlantic basin (Fig. 4, top row) and a westward shift of the large-scale monsoon divergence circulation in the Eastern Hemisphere, shifting the corresponding Rossby wave response further west. At low levels, the NASH is also displaced westward (Fig. 4, 2nd row), accompanied by deep layer subsidence (Fig. 4, 3rd row) in the western Atlantic (~100-60°W) in a manner consistent with related work using similar experiments (SV16).

Subtropical rainfall changes in the PATCH experiments (Fig. 4, bottom row) follow these zonal shifts in the stationary wave circulation and closely resemble the multi-model mean CMIP5 response (Fig. 1). Monsoon precipitation in the Eastern Hemisphere is preferentially increased over land and decreased over the ocean, and a westward displaced NASH yields low-level moisture divergence and drying on its western edge (Fig. 4). Drying in the western Atlantic in the PATCH experiments is thus driven by changes in the stationary eddy atmospheric circulation, not moisture field, again consistent with the CMIP5 response to global forcing (Figs. 3 and S7).

5. Summary and Discussion

A local patch of radiative forcing over land near North Africa reproduced the total pattern of the response to global forcing in CAM4/CCSM4 mid-Holocene and AMIP4xCO_2 experiments. This imposed energy anomaly drives an enhancement of the broad-scale Afro-Asian monsoon, with increased continental rainfall and a distinct westward displacement of the monsoon divergent circulation and subtropical high. Remote heating of land is thus the common driver of a westward displaced NASH and drying in the Atlantic under increased CO_2 and insolation. The similarity across uncoupled CO_2 and coupled insolation PATCH experiments highlights the central role of a TOA perturbation over land in constraining the pattern of circulation and rainfall changes in the Atlantic. However, other mechanisms need to be considered in quantifying the amplitude of changes. For instance, the relatively weaker rainfall response in the coupled mid-Holocene simulations (Fig. 4, bottom row) despite comparable TOA forcing (Fig. 4, top row), may point to the competing role of SST feedbacks and ocean circulation changes on the stationary wave response to radiative forcing (Shaw and Voigt, 2015). Still, we anticipate the principal results found here to be relevant to more realistic climate change scenarios with associated SST warming, since changes in the NASH wind field ultimately govern drying in the Atlantic (Fig. 3) and a westward displaced NASH is a common result of prescribed-SST AMIP4xCO2 *and* coupled rcp8.5 experiments (see Figure 1 of Shaw and Voigt, 2015).

Unlike regions of projected increased precipitation, where the 'wet-get-wetter' paradigm is a reasonable approximation of the response to CO_2 forcing (Held and Soden, 2006), subtropical *drying* in future climate change projections have been shown to be inconsistent with thermodynamic scaling arguments and independent of changes in SST and zonal mean subsidence (He and Soden, 2017). This implies the importance of the stationary wave circulation–driven by land-sea heating asymmetries–in governing regional-scale drying under CO_2 increase. And as demonstrated above, drying during the Mid-Holocene was also driven by similar changes in the stationary wave circulation under increased insolation over land. Consistent mechanistic reasoning applies when interpreting summer drying in the western Atlantic in response to direct CO_2 warming and direct insolation warming.

Our findings extend recent work by Shaw and Voigt (2015, 2016) and suggest that the principal remote response in the North Atlantic to a climate perturbation is not particularly sensitive to the details of the radiative forcing, so long as the forcing includes robust energy input over land near North Africa. This increased energy input appears to act as a moist amplification process near arid regions on the margin of existing monsoons in CAM4/CCSM4, causing an increase in continental monsoon rainfall and a westward shift of the broad-scale subtropical circulation. In looking at inter-model differences across the CMIP5 ensemble, there is also a correlation between increased monsoon rainfall and the circulation response to 4xCO2 in the western Atlantic (Fig. S8), consistent with the observed relationship found in inter-annual samples (Kelly and Mapes, 2011). This may also point to the role of moist heating in amplifying the total response to external radiative forcing.

One caveat in interpreting our results, however, is that the moist-coupled response of CAM4/CCSM4 exhibits excessive precipitation near North Africa as compared to the CMIP5 multi-model mean (compare Figs. 1 and S4). While such a westward amplification of latent heating in the PATCH region may amplify the westward shift of the NASH, it need not be a necessary condition. Atmosphere energy input over land near North Africa might also directly drive changes in the divergent circulation and coupled Rossby wave via the increase in dry static energy there (as discussed in SV16). It may be fruitful to further disentangle the role of dry vs moist heating processes on the resultant moist-coupled circulation response of such experiments in future work.

The role of monsoons in governing the climatological summertime subtropical anticyclones is well known (e.g. Rodwell and Hoskins, 2001), and a monsoon-driven westward shift of the NASH has previously been shown to cause climatological drying on sub-seasonal to seasonal timescales (Kelly and Mapes, 2011, 2013, Shaw and Voigt, 2015). Similar atmosphere dynamics appear relevant to simulated mid-Holocene precessional changes and the 4xCO2 forcing scenario considered here, lending confidence to the role of remote radiative heating on governing the North Atlantic circulation and rainfall response in summer. Westward shifts of the NASH in warmer climates may also have important implications on tropical cyclone tracks in the Atlantic, perhaps helping to explain secular variations of land-falling events in the paleo record (Elsner et al., 2000).

By highlighting common physical linkages of the climate system, this study helps to unify interpretation of regional rainfall changes across a variety of forcing constraints. Remote heating of Afro-Asia is a common cause of drying of the America-Atlantic region in summer, independent of whether the climate system is forced by annual cycle insolation changes, orbital precessional changes, or CO_2 increase. Understanding subtropical circulation and rainfall changes in light of the highly repeatable and observable seasonal cycle may thus be a useful lens through which to interpret climate change projections.

Acknowledgments

This work was supported by the Office of Science of the U.S. Department of Energy (DOE) Biological and Environmental Research as part of the Regional and Global Climate Modeling Program. The Pacific Northwest National Laboratory is operated for DOE by Battelle Memorial Institute under contract DE-AC05-76RL01830. This work used computing resources provided by the National Energy Research Scientific Computing Center (NERSC), a DOE Office of Science User Facility supported by the Office of Science of the U.S. Department of Energy under Contract No. DE-AC02-05CH11231.The CAM4/CCSM4 simulations are archived at NERSC and are available upon request (*patrick.kelly@pnnl*.gov). The CMIP5 data used in this study is publicly available (https://esgf-node.llnl.gov/). P.K. is also grateful for discussions with Brian Mapes and comments from two anonymous reviewers whose efforts significantly improved this manuscript.

Author contributions

P.K. designed the research and led the writing. P.K. and B.K. conducted the experiments. All authors analyzed and discussed the results and contributed to the writing.

Competing financial interest

The authors declare no competing financial interests.

References

Allen, M.R., and W. J. Ingram (2002) Constraints on future climate and the hydrological cycle. *Nature*, 419, 224-232.

Chen, J., & Bordoni S. (2014). Orographic effects of the Tibetan Plateau on the East Asian Summer monsoon: An energetic perspective. *J. Climate*, 27, 3052–3072.

Chen, P., Hoerling, M. P., & Dole, R. M. (2001). The origin of the subtropical anticyclones. *J. Atmos. Sci*. **58**, 1827–1835.

Colbert, A. J. & Soden, B. J. (2012). Climatological variations in North Atlantic tropical cyclone tracks. *J. Clim.* **25**, 657–673.

Elsner, J. B., Liu, K. B. & Kocher, B. (2000). Spatial variations in major US hurricane activity: Statistics and a physical mechanism. *J. Clim.* **13**, 2293–2305.

Gent, P. R., & Coauthors (2011). The Community Climate System Model version 4. *J. Climate* **24**, 4973–4991.

Grimm, E. C. & Coauthors (1993). A 50,000-year record of climate oscillations from Florida and its temporal correlation with the Heinrich events. *Science* **261**,198–200.

Harrison, S. P. & Coauthors (2015). Evaluation of CMIP5 palaeo-simulations to improve climate projections. *Nat. Clim. Change* **5,** 735–743.

He, J. & Soden, B. J. (2017). A re-examination of the projected subtropical precipitation decline. *Nat. Clim. Change* **7**, 53–57.

Held, I. M. & Soden, B. J. (2006). Robust responses of the hydrological cycle to global warming. *J. Clim.* **19,** 5686–5699.

Hoskins, B. J., & Rodwell, M. J. (1995). A model of the Asian summer monsoon. Part I: The global scale. *J. Atmos. Sci.* **52**, 1329–1340.

IPCC *Climate Change 2013: The Physical Science Basis* (eds Stocker, T. F. *et al.*) (Cambridge Univ. Press, 2013).

Jolly, D. & Coauthors (1998). Biome reconstruction from pollen and plant macrofossil data for Africa and the Arabian peninsula at 0 and 6000 years. *J. Biogeogr.* **25,** 1007–1027.

Kelly, P., & Mapes, B. (2011). Zonal mean wind, the Indian monsoon, and July drying in the western Atlantic subtropics. *J. Geophys. Res*. **116**.

—, & —. Asian monsoon forcing of subtropical easterlies in the Community Atmosphere Model: Summer climate implications for the western Atlantic. (2013). *J. Clim.* **26**, 2741–2755.

Levine X. J., and Boos W. R. (2016). A mechanism for the response of the zonally asymmetric subtropical hydrologic cycle to global warming. Journal of Climate, 29, 7851-7867.

Mantsis, D. F., Clement, A. C., Kirtman, B. P., Broccoli, A. J, & Erb M. P. (2013). Precessional cycles and their influence on the North Pacific and North Atlantic summer anticyclones. *J. Clim.* **26**, 4596–4611.

Merlis, T. M. (2015). Direct weakening of tropical circulations from masked CO_2 radiative forcing. *Proc. Natl. Acad. Sci.* **112**, 13167–13171.

Miyasaka, T., & Nakamura H. (2005). Structure and formation mechanisms of the Northern Hemisphere summertime subtropical highs. *J. Clim.* **18**, 5046–5065.

Neale, R. B., & Coauthors (2011). Description of the NCAR Community Atmosphere Model (CAM4). NCAR Tech. Note NCAR/TN-485+STR, 120 pp.

Neelin, J. D., and I. M. Held (1987). Modeling tropical convergence based on the moist static energy budget. *Mon. Wea. Rev.*, **115**, 3–12.

Nie, J., W. Boos, and Z. Kuang, (2010). Observational evaluation of a convective quasi-equilibrium view of monsoons. *J. Climate*, **23**, 4416–4428.

Overpeck, J., Anderson, D., Trumbore, S. & Prell, W. (1996). The southwest Indian Monsoon over the last 18,000 years. *Clim. Dynam.* **12**, 213–225.

Perez-Sanz, A., Li, G., Gonzalez-Samperiz, P. & Harrison, S. P. (2014). Evaluation of modern and mid-Holocene seasonal precipitation of the Mediterranean and northern Africa in the CMIP5 simulations. *Clim. Past* **10,** 551–568.

Rodwell, M. J., & Hoskins, B. J. (1996). Monsoons and the dynamics of deserts. *Quart. J. Roy. Meteor. Soc.* **122**, 1385–1404.

Rodwell, M. J., & Hoskins, B. J. (2001). Subtropical anticyclones and summer monsoons. *J. Clim.* **14**, 3192–3211.

Seager, R., Naik, N. & Vecchi, G. A. (2010). Thermodynamic and dynamic mechanisms for large-scale changes in the hydrological cycle in response to global warming. *J. Clim.* **23**, 4651–4668.

Shaw, T. A., & Voigt A. (2015). Tug of war on summertime circulation between radiative forcing and sea surface warming. *Nat. Geosci.* **8**, 560–566.

Shaw, T. A., & Voigt A. (2016). Land dominates the regional response to CO_2 direct radiative forcing. *Geophys. Res. Lett.,* **43**, 11,383-11,391.

Shin, S. I., Sardeshmukh, P. D., Webb, R. S., Oglesby, R. J. & Barsugli J. J. Understanding the mid-Holocene climate. (2006). *J. Clim.* **19**, 2801–2817.

Taylor, K. E., Stou er, R. J. & Meehl, G. A. (2012). An overview of CMIP5 and the experiment design. *Bull. Am. Meteorol. Soc.* **93,** 485–498.

Ting, M. Maintenance of northern summer stationary waves in a GCM. (1994). *J. Atmos. Sci.* **51**, 3286–3308.

Wills, R. C., M. P. Byrne, and T. Schneider. (2016). Thermodynamic and dynamic controls on changes in the zonally anomalous hydrological cycle. *Geophys. Res. Lett.*, **43**, 4640-464.

FIGURE LIST:

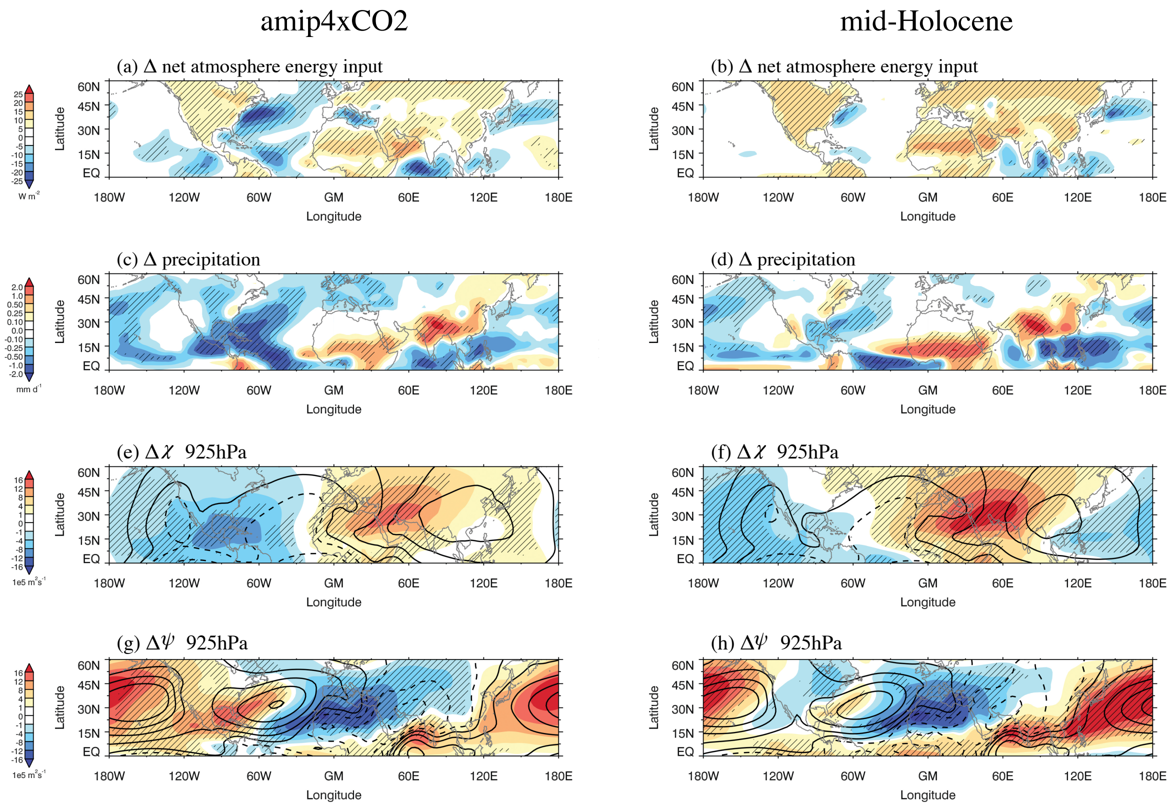

Figure 1: JJA multi-model ensemble mean difference (colors) of net atmosphere energy input (a,b), precipitation (c,d), and low-level velocity potential (e,f) and zonally asymmetric stream function (g,h) for AMIP4xCO_2 minus AMIP (left) and mid-Holocene minus piControl (right). Background control climatology of velocity potential and stream function is indicated by the thick black contours in (e-h) with solid and dashed contours indicating positive and negative values, respectively, with the zero contour omitted. Cross-hatching indicates >80% model agreement on the sign of the change (i.e. robustness). Net atmosphere energy input is defined as the difference of TOA minus surface fluxes (Methods).

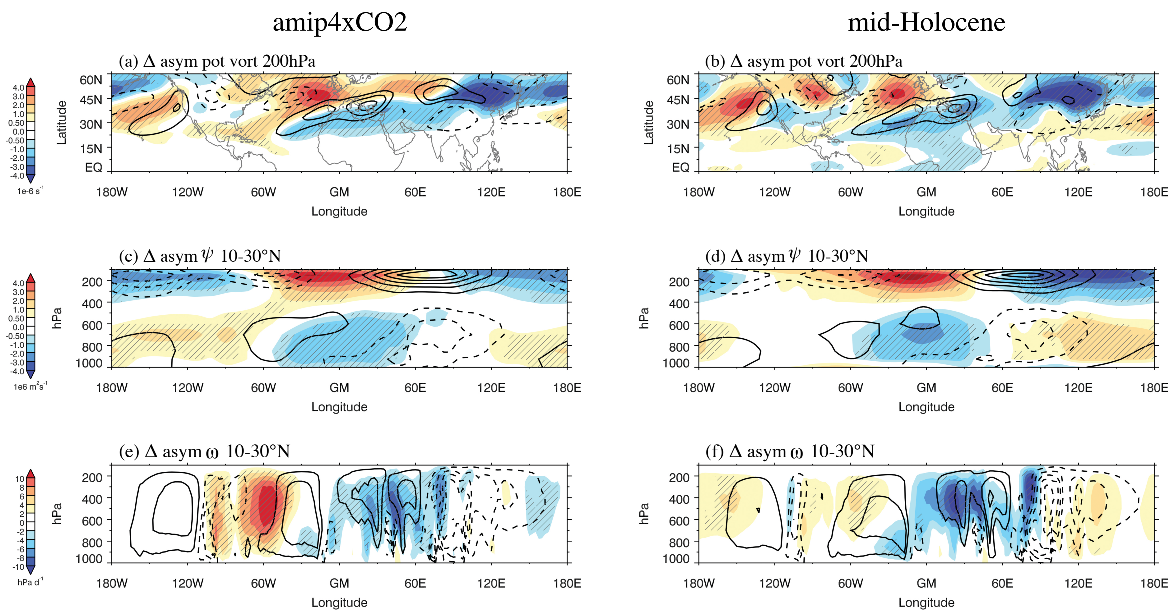

Figure 2: JJA multi-model ensemble mean difference (colors) of asymmetric upper level potential vorticity (top), stream function (middle), and pressure velocity (bottom) for AMIP4xCO_2 minus AMIP (left) and mid-Holocene minus piControl (right). Contouring and cross-hatching convention as in Fig.1.

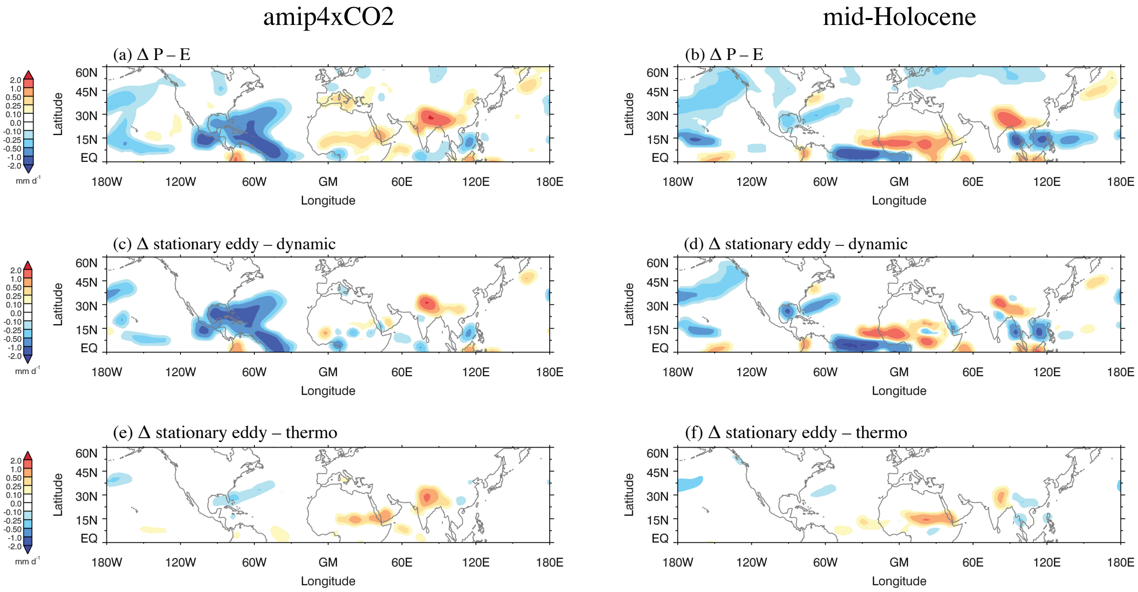

Figure 3: JJA multi-model ensemble mean moisture budget for AMIP4xCO_2 minus AMIP (left) and mid-Holocene minus piControl (right). The ‘dynamic’ term (c,d) involves change in the stationary eddy wind against the background moisture field, i.e. $-\langle \nabla \cdot (\delta\overline{\boldsymbol{v}}^{*} \cdot \overline{q})\rangle$. The ‘thermodynamic’ term (e,f) involves changes in moisture field against the background stationary eddy wind, i.e. $-\langle \nabla \cdot (\delta\overline{\boldsymbol{v}}^{*} \cdot \overline{q})\rangle$. See Methods for details. Only grid points where models show robust agreement (>80%) on the sign change of $P - E$ are plotted.

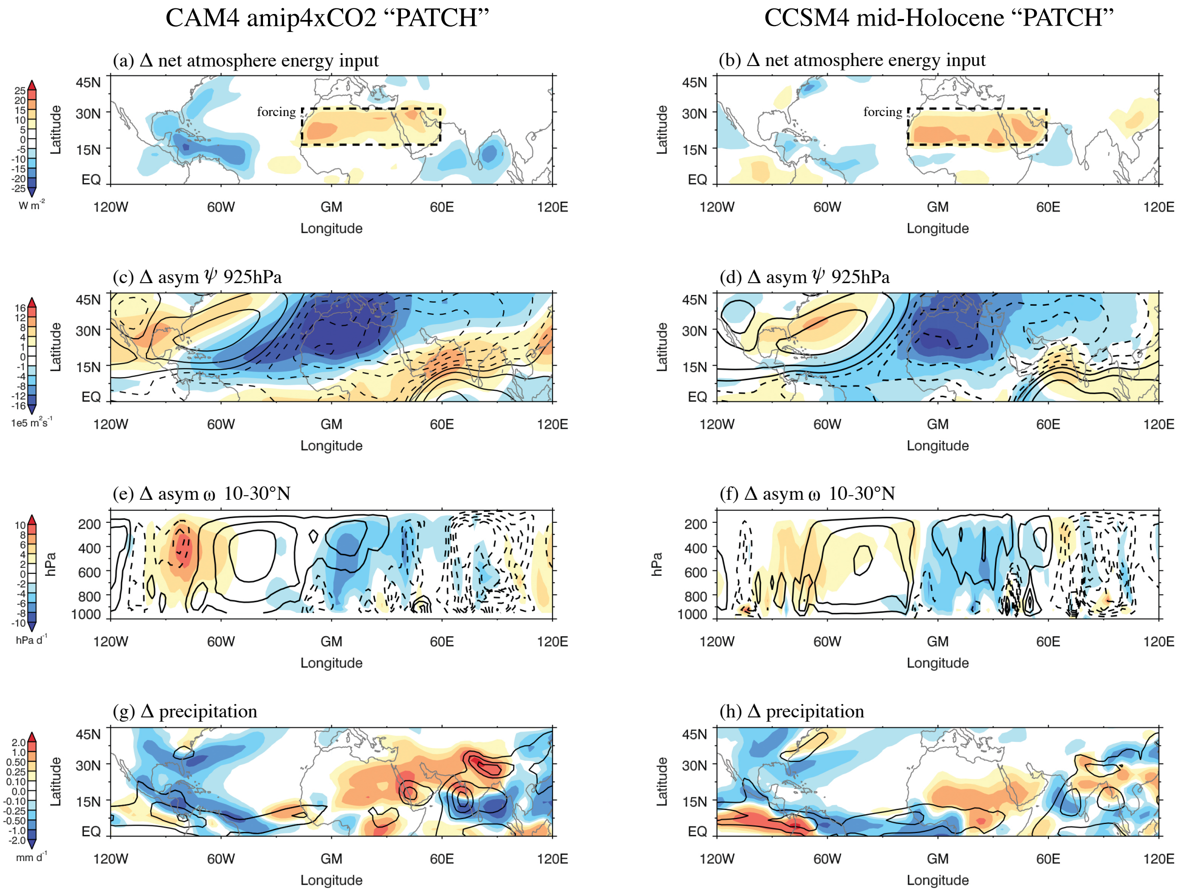

Figure 4: JJA mean difference of indicated fields (colors) for CAM4_AMIP4xCO_2_PATCH minus CAM4_AMIP (left) and CCSM4_mid-Holocene_patch minus CCSM4_piControl (right), overlaid with contours of background control climatology in (c-h) using same convention as Figs. 1-2. PATCH experiments are forced by the respective CO_2 and insolation increases only over the region indicated by the dashed black rectangle in (a,b).